
GOAL INFERENCE WITH RAO-BLACKWELLIZED PARTICLE FILTERS*

Yixuan Wang^{1†}, Dan P. Guralnik², Warren E Dixon¹

¹Department of Mechanical and Aerospace Engineering, University of Florida

²Department of Mathematics, Ohio University

wang.yixuan, wdixon@ufl.edu

danguralnik@ohio.edu

ABSTRACT

Inferring the eventual goal of a mobile agent from noisy observations of its trajectory is a fundamental estimation problem. We initiate the study of such intent inference using a variant of a Rao–Blackwellized Particle Filter (RBPF), subject to the assumption that the agent’s intent manifests through closed-loop behavior with a state-of-the-art provable practical stability property. Leveraging the assumed closed-form agent dynamics, the RBPF analytically marginalizes the linear-Gaussian substructure and updates particle weights only, improving sample efficiency over a standard particle filter. Two difference estimators are introduced: a Gaussian mixture model using the RBPF weights and a reduced version confining the mixture to the effective sample. We quantify how well the adversary can recover the agent’s intent using information-theoretic leakage metrics and provide computable lower bounds on the Kullback–Leibler (KL) divergence between the true intent distribution and RBPF estimates via Gaussian-mixture KL bounds. We also provide a bound on the difference in performance between the two estimators, highlighting the fact that the reduced estimator performs almost as well as the complete one. Experiments illustrate fast and accurate intent recovery for compliant agents, motivating future work on designing intent-obfuscating controllers.

Keywords Estimation and filtering · Kalman filtering

1 Introduction

Motivation. Anticipating an agent’s goals from partial, noisy observations is central to safe autonomy and human–robot interaction. Intent inference supports early decision making by allowing robots to reason over multiple plausible futures before conflicts arise, which is critical in navigation, assistance, and surveillance settings. The problem is intrinsically uncertain because the latent goal and arrival time induce distinct families of trajectories that often overlap in early observations.

Intent inference and obfuscation have been studied extensively in discretized environments, where the environment is modeled as a finite graph or Markov decision process (MDPs) and high-level tasks are expressed in temporal logics [1, 2, 3]. In stochastic settings, entropy-maximizing policies and task-aware planning in MDPs have been used to minimize the predictability of trajectories or to limit the information leaked about high-level task specifications [4, 5]. A complementary line of work leverages differential privacy to bound what an adversary can infer from observed paths, either by privatizing transition probabilities or by enforcing privacy at the level of symbolic trajectories and Markov chains [6, 7, 8]. These approaches typically operate on finite-state abstractions of the underlying dynamics and, apart from recent formulations of entropy-based obfuscation in partially observable models [9], offer limited guidance on how to perform intent inference directly in continuous state spaces with nonlinear dynamics.

*This research was supported in part by Air Force Office of Scientific Research award number FA9550-22-1-0429. Any opinions, findings and conclusions or recommendations expressed in this material are those of the author(s) and do not necessarily reflect the views of the sponsoring agency.

†Corresponding author.

Particle filters propagate weighted hypotheses of latent variables under nonlinear, non-Gaussian dynamics, but their performance degrades as state dimension grows. RBPF [10] addresses this difficulty by exploiting model structure: it samples a subset of the variables while analytically marginalizing the remainder using finite-dimensional optimal filters, thereby reducing variance and improving sample efficiency. Its effectiveness has been demonstrated in tracking and simultaneous localization and mapping [11] as well as in multiple-target data association, where conditional linear-Gaussian substructures are common.

Contributions. This work develops an RBPF formulation for agent intent inference. The model treats intent θ as a tuple (goal location x , goal radius r , arrival time t) and uses assumed closed-loop dynamics with bounded unknown disturbance to induce a conditionally linear-Gaussian evolution of the observed state. Only the intent parameters are sampled, while analytically propagating the kinematic state. Particle weights are updated from trajectory observations via a Kalman update, concentrating the Monte Carlo effort on the latent intent.

Two estimators representing intent as a distribution over the space of intent parameters are developed, representing weighted averages of the evolving set of particles, with and without pruning away ineffective particles. A bound on the difference in information leakage between the two estimators is established. Finally, numerical experiments indicate fast, accurate intent recovery in nominal conditions, with performance degrading gracefully under measurement noise.

2 Problem Formulation

We consider two principal entities, an adversary and an agent, whose positions evolve in \mathbb{R}^n , $n \in \{2, 3\}$, corresponding to planar ($n = 2$) or spatial ($n = 3$) motion. The agent's intent is specified by a triple $\theta^* \triangleq (x^*, r^*, t^*)$, where $x^* \in \mathbb{R}^n$ is the goal center, $r^* > 0$ is the goal radius, and $t^* > 0$ is the desired arrival time; the corresponding goal set is the ball $x^* + r^* \mathbb{B}$, which the agent aims to reach by time t^* . The adversary's objective is to infer the intent parameter θ^* by observing the agent's trajectory. The adversary is assumed to be a passive observer, focusing the analysis on the agent's control decisions aimed at obscuring θ^* from the adversary. The values of θ^* are confined to the domain

$$\Theta \triangleq R\mathbb{B} \times [r_{\min}, r_{\max}] \times [T_{\min}, T_{\max}], \quad (1)$$

where $R > 0$, $0 < r_{\min} \ll r_{\max} \ll R$, and $0 < T_{\min} \ll T_{\max}$ are parameters of the problem, fixed in advance. Define mappings $x(\theta) : \Theta \rightarrow \mathbb{R}^n$, $r(\theta) : \Theta \rightarrow \mathbb{R}$ and $t(\theta) : \Theta \rightarrow \mathbb{R}$ such that, for each $\theta \in \Theta$, the quantities $x(\theta)$, $r(\theta)$ and $t(\theta)$ denote the goal center, radius, and arrival time associated with intent θ . The notation $\theta = (x(\theta), r(\theta), t(\theta))$ for $\theta \in \Theta$ will be used when there is no risk of ambiguity.

While the adversary may observe the agent and have knowledge of the agent dynamics, the control input values deployed by the agent are typically unavailable in real time to any outside observer. However, information regarding the dependency of the controllers on the agent's task may be available, enabling the inference of the agent's goal from observations of its closed-loop behavior. It is also reasonable for the adversary to assume that the closed loop dynamics of the agent, while possibly noisy, is designed to stabilize the goal within the allotted time. Letting $\hat{\theta}$ denote the estimate of θ^* by the adversary, these considerations may be cast into the following assumption.

Assumption 1. Given $\theta \in \Theta$, if $\hat{\theta} = \theta$ then the adversary estimates the closed-loop dynamics of the agent as

$$\dot{\hat{x}} \in \underbrace{-\lambda(\theta)(\hat{x} - x(\theta))}_{\triangleq f_\theta(\hat{x})} + \bar{d}\mathbb{B}, \quad (2)$$

where $\lambda : \Theta \rightarrow (0, \infty)$ is determined according to Lemma 1.

The parameter \bar{d} in (2) represents an upper bound on the sum-total of unknown disturbances to the closed-loop dynamics f_θ . It is reasonable to assume this bound is known to the adversary, representing some knowledge of the agent's system capabilities in the environment.

Lemma 1. Let $\theta \in \Theta$ and let $x \in \mathbb{R}^n$ evolve under

$$\dot{x} \in -\lambda(x - x(\theta)) + \bar{d}\mathbb{B}. \quad (3)$$

Then for any $\lambda \geq \lambda_\theta$, and any $x_0 \in R\mathbb{B}$, the trajectory emanating from $x(0) = x_0$ satisfies $x(t) \in x(\theta) + r(\theta)\mathbb{B}$ for all $t \geq t(\theta)$, where:

$$\lambda_\theta \triangleq \max \left\{ \frac{\bar{d}}{r(\theta)}, \frac{1}{t(\theta)} \log \frac{R}{r(\theta)} \right\}. \quad (4)$$

Proof. See Appendix A. □

Using the behavior model of the agent provided by (2) and Lemma 1 (specifically, with $\lambda(\theta) = \lambda_\theta$), the adversary seeks to infer the true intention θ^* from real-time observations of the agent's state.

3 Intention Inference

Unlike the standard PF, our work employs a RBPF to accelerate the Monte-Carlo process [12], tailored specifically for the intention inference scenario. Specifically, by Assumption 1, applying a Kalman Filter to the agent state-estimates corresponding to each particle instead of using the full Monte Carlo update reduces the computation load. However, in the developed method, the particles will represent intent, rather than state. Hence, they are not propagated through the filtering process, but the particle weights are updated at each timestep based on the discrepancy between the observed trajectory and the simulated trajectories generated by each particle.³

3.1 RBPF Model Development

We employ a set of $N \gg 1$ weighted particles $(\theta_k^{(i)}, \omega_k^{(i)})_{k=0, i=1}^{\infty, N}$ to recursively estimate the intent parameter θ^* from incoming data. The initialization prior for the particles is uniform over Θ . Denote $x_k^{(i)} \triangleq x(\theta_k^{(i)})$, $r_k^{(i)} \triangleq r(\theta_k^{(i)})$, and $t_k^{(i)} \triangleq t(\theta_k^{(i)})$ for all $k \geq 0$ and $1 \leq i \leq N$. The adversary's noisy observation of the position of the agent at time t_k is modeled as

$$y_k - x(t_k) \sim \mathcal{N}(0, \Delta),$$

where $\mathcal{N}(0, \Delta)$ is the zero mean Gaussian distribution with symmetric positive-definite covariance Δ . Each particle represents a possible evolution, $(\hat{x}_k^{(i)})_{k=0}^{\infty}$, of the agent's trajectory, given the assumed dynamics $f_k^{(i)} \triangleq f_{\theta_k^{(i)}}(\hat{x}_k^{(i)})$, provided in (2), with the associated gain $\lambda_k^{(i)} \triangleq \lambda(\theta_k^{(i)})$. These considerations motivate the following Bayesian filtering procedure.

Initialization. The N particles are assigned uniform weights, $\omega_0^{(i)} \triangleq 1/N$, with the points $x_0^{(i)}$ sampled uniformly from the workspace Ω ; the radii $r_0^{(i)}$ sampled uniformly from a pre-defined interval $[r_{\min}, r_{\max}]$; and the times $t_0^{(i)}$ sampled uniformly from the pre-defined interval $[T_{\min}, T_{\max}]$. The initial state estimate corresponding to each particle i is set to the initial measurement, $\hat{x}_0^{(i)} := y_0$.

Propagation Step: Discrete Euler integration of the dynamics (2) provides a non-deterministic transition model⁴ of particle i for timestep k yielding the prior $\hat{x}_k^{(i-)}$

$$\hat{x}_k^{(i-)} - \hat{x}_{k-1}^{(i)} - \Delta t_k f_{k-1}^{(i)} \in \Delta t_k (\bar{d}\mathbb{B}). \quad (5)$$

To obtain a probabilistic transition model, the disturbance term in (5) is modeled as Gaussian noise

$$\hat{x}_k^{(i-)} - \hat{x}_{k-1}^{(i)} - \Delta t_k f_{k-1}^{(i)} \sim \mathcal{N}(0, \Delta t_k^2 \Sigma) \quad (6)$$

where $\Sigma \triangleq (\sigma \bar{d})^2 \mathbf{I}_n$ and $\sigma > 0$ is a user-selected parameter determining the tail of the disturbance outside the ball $\bar{d}\mathbb{B}$. The prior error covariance \mathbf{P}_k^- then equals

$$\mathbf{P}_k^- = (\lambda_{k-1}^{(i)})^2 \mathbf{P}_{k-1} + \Sigma, \quad (7)$$

and the Kalman gain \mathbf{K}_k is updated to

$$\mathbf{K}_k = \mathbf{P}_k^- (\mathbf{P}_k^- + \Delta)^{-1}, \quad (8)$$

yielding the state posterior $\hat{x}_k^{(i)}$ and the posterior error covariance \mathbf{P}_k

$$\hat{x}_k^{(i)} = \hat{x}_k^{(i-)} + \mathbf{K}_k (y_k - \hat{x}_k^{(i-)}), \quad \mathbf{P}_k = (I - \mathbf{K}_k) \mathbf{P}_k^-. \quad (9)$$

Update Step. The new measurement y_k of the agent's position $x(t_k)$ causes an update of the particle weights as

$$\omega_k^{(i)} \propto \omega_{k-1}^{(i)} p(y_k | \hat{x}_k^{(i)}), \quad p(y_k | \hat{x}_k^{(i)}) \sim \mathcal{N}(\hat{x}_k^{(i)}, \Delta), \quad (10)$$

followed by a normalization of the weights.

Resampling Step. Following a number of iterations, many particles could carry negligible weights, wasting computational resources. To counter this problem, the effective sample size N_{eff} is defined by

$$N_{\text{eff}} \triangleq \left\lfloor \left(\sum_{i=1}^N (\omega_k^{(i)})^2 \right)^{-1} \right\rfloor. \quad (11)$$

³Note that, as a result, a large number of particles is needed, to obtain a representative sample of Θ .

⁴Note that this is the only place where f_θ comes to bear on the RBPF. Therefore, in principle, the developed framework may be applied for other assumed agent dynamics.

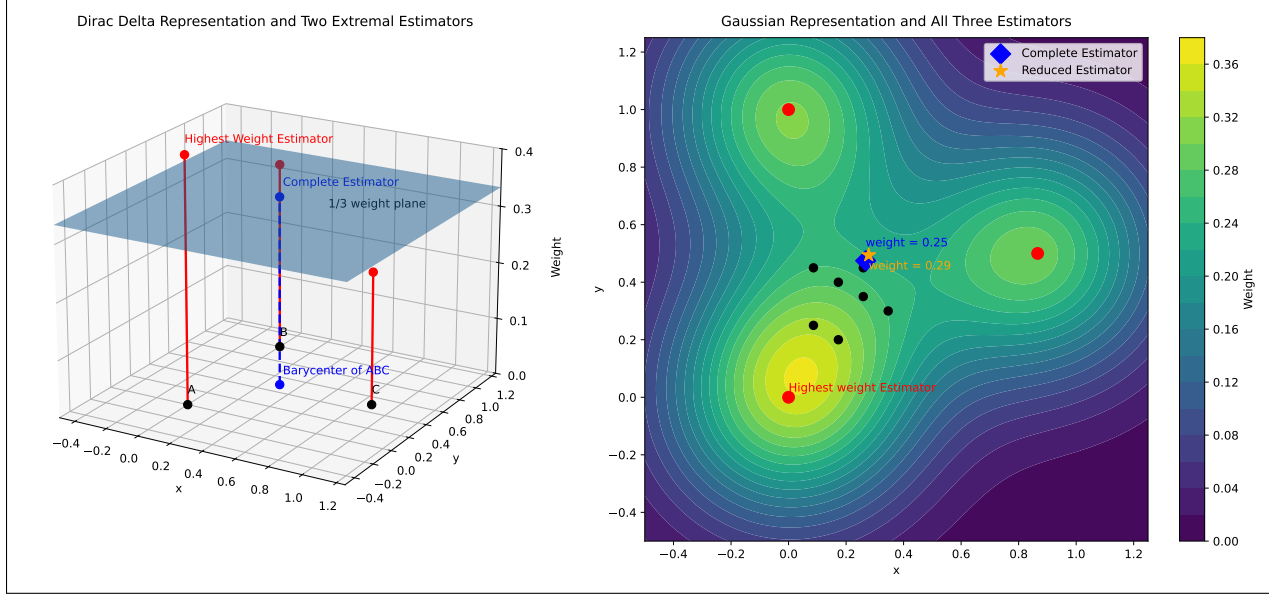


Figure 1: **Left:** Hypothetical situation with three particles estimating $x(\theta^*)$ with near-equal weights. The particle A with weight $\frac{1}{3} + \varepsilon$, is a highest weight estimate of θ^* according to the PF, but it represents a false positive with high probability ($\frac{2}{3} - \varepsilon$). At the same time, the weighted average of the particles may not be relevant at all, since its location is not contained in *any* of the predicted goal regions. **Right:** Hypothetical situation with three effective particles with near-equal weights $\omega = 0.29$, represented by the reduced estimator (in distribution form), in Section 3.2.3. Seven additional particles with negligible weights are located near the barycenter of the three effective particles. Similar to Dirac representation, the highest weight estimator remains a false positive with high probability. The position estimate from the weighted average of all particles $x(\hat{\theta}_k^{\text{com}})$ is distracted by the trivial weight particles, while the reduced estimator stays at the barycenter of effective particles with weight almost equal to the effective particles' weight. However, in contrast to Dirac representation, either estimator provides information about the goal distribution q_{θ^*} .

When N_{eff} drops below a predefined threshold N_0 , we retain the N_0 highest weight particles and discard those with negligible weights. The retained particles $(\theta_k^{(i_a)}, \omega_k^{(i_a)})_{a=1}^{N_0}$ are then replicated in proportion to their relative weights. That is, each particle $(\theta_k^{(i_a)}, \omega_k^{(i_a)})$ is replaced with $N_a \triangleq \left\lfloor \omega_k^{(i_a)} N / \sum_{b=1}^{N_0} \omega_k^{(i_b)} \right\rfloor$ particles of weight $\frac{1}{N}$ and position $\theta_k^{(i_a)}$. The remaining $N - \sum_{b=1}^{N_0} N_b$ particles are re-initialized in random positions in Ω with weights equal to $\frac{1}{N}$, to contribute to better coverage of the search space.

Remark 1. *It is important to note that $\theta_{k+1}^{(i)} = \theta_k^{(i)}$ unless the i -th particle is discarded during resampling. In other words, the intent parameter attached to any particle is held constant throughout the particle's lifetime.*

3.2 Estimation and Inference

The weight update law of the RBPF may motivate the adoption of either the highest weight particle, or the weighted average of the effective particles, as estimates of the agent's true goal, θ^* . This approach, however, is ineffectual for the purpose of inferring intent, as discussed in Figure 1, calling for a more rigorous approach to estimation which enables quantifying the amount of information about θ^* gained from the estimator.

3.2.1 Representation of Intent by a Distribution

At any point $t = t_k$ in time, the N weighted particles $(\theta_k^{(i)}, \omega_k^{(i)})_{i=1}^N$ may be used to give rise to estimators of θ^* . Any such estimator, ultimately, is a random variable, which may be regarded as a measurement of θ^* . Thus, each $\theta \in \Theta$ ought to be represented by a probability density q_θ over Θ with mean θ . Following our earlier convention, denote $q_k^{(i)} \triangleq q_{\theta_k^{(i)}}$, for simplicity. For computational simplicity, the q_θ are selected as continuous distributions⁵ over $\tilde{\Theta} \triangleq \mathbb{R}^n \times (0, \infty)^2$, obtained as products of the form

$$q_\theta \sim \mathcal{N}(x(\theta), \sigma_x^2 \mathbf{I}_n) \otimes \mathcal{R} \otimes \mathcal{T}, \quad \log(\mathcal{R}) = \mathcal{N}(r(\theta), \sigma_r^2), \quad \log(\mathcal{T}) = \mathcal{N}(t(\theta), \sigma_t^2), \quad (12)$$

⁵Returning to the initial considerations of Section 3.2, note also that selecting q_θ to be a Dirac distribution would not allow for evaluating the amount of information about θ^* present in q_θ .

where $\sigma_x, \sigma_r, \sigma_t$ are system parameters representing the capacity of the adversary for precise localization and timing and guaranteeing that an overwhelming probability is assigned to the event $\Theta \subset \tilde{\Theta}$.

In computations, the marginal probability density functions of q_θ will be denoted by $[q_\theta]_x, [q_\theta]_r$ and $[q_\theta]_t$, respectively.

3.2.2 Density-Based Estimators of Intent

Replacing the PF with its associated collection of distributions $(q_k^{(i)})_{i=1}^N$ allows for the construction of analogous, yet more meaningful estimators, $\hat{\theta}_k \triangleq \mathbb{E}[\hat{q}_k]$, where the probability distributions \hat{q}_k over $\tilde{\Theta}$ are constructed as follows:

Highest Weight Estimator. The highest weight estimator corresponds to selecting $\hat{q}_k = q_k^{(i_0)}$, where $i_0 = \arg \max_i \omega_k^{(i)}$. Note that it is now possible to quantify the discrepancy between θ^* and $\hat{\theta}_k$ using KL-divergence, as follows. Denote $\hat{x}_k \triangleq x(\hat{\theta}_k), \hat{r}_k \triangleq r(\hat{\theta}_k)$, and $\hat{t}_k \triangleq t(\hat{\theta}_k)$ for all $k \geq 0$. Then,

$$D_{KL}(q_{\theta^*} \parallel \hat{q}_k) = \sum_{\nu \in \{x, r, t\}} D_{KL}([q_{\theta^*}]_\nu \parallel [q_{\hat{\theta}_k}]_\nu) = \frac{\|x^* - \hat{x}_k\|^2}{2\sigma_x^2} + \frac{(r^* - \hat{r}_k)^2}{2\sigma_r^2} + \frac{(t^* - \hat{t}_k)^2}{2\sigma_t^2}.$$

However, this estimator still suffers from the same drawback that was pointed out in Figure 1.

Complete Estimator. The challenges raised in Figure 1 are resolved through weighted averaging of the representative distributions of the particles (rather than the particles themselves), namely:

$$\hat{q}_k^{\text{com}} \triangleq \sum_{i=1}^N \omega_k^{(i)} q_k^{(i)}, \quad (13)$$

noting that although $\hat{\theta}_k = \sum_{i=1}^N \omega_k^{(i)} \theta_k^{(i)}$, the distribution \hat{q}_k rarely satisfies $\hat{q}_k = q_{\hat{\theta}_k}$ (see Figure 1). This discrepancy emphasizes the fact that it is \hat{q}_k that contains the most information about θ^* rather than just its first moment, motivating the study of bounds on $D_{KL}(q_{\theta^*} \parallel \hat{q}_k)$.

3.2.3 The Reduced Estimator

Since ineffective particles are discarded in the resampling stage of the PF update, their contribution being minuscule, it is reasonable to maintain a reduced estimator of the form

$$\hat{q}_k^{\text{red}} \triangleq \sum_{i \in \mathcal{M}_k} \frac{\omega_k^{(i)}}{\omega_{\text{eff}}} q_k^{(i)}, \quad (14)$$

where the set $\mathcal{M}_k \subseteq \mathcal{P}$ is the set of the N_{eff} highest weight particles and the set \mathcal{P} is defined as the set of all particles, and $\omega_{\text{eff}} = \sum_{i \in \mathcal{M}_k} \omega_k^{(i)}$. The right subplot of Figure 1 gives an intuitive representation of the three estimators, from which the top N_{eff} representation contains the maximum information among all three. Then, $\hat{\theta}_k^{\text{com}}$ and $\hat{\theta}_k^{\text{red}}$ denote the intent estimates at time step k defined as the expectations of the complete and reduced estimators, respectively.

4 Intent Estimators: Reduced vs. Complete

Let H_k^{com} and H_k^{red} denote the information leakage from the true intent distribution to the estimated one at time step k using the average estimator and the reduced estimator, respectively,

$$H_k^{\text{com}} \triangleq D_{KL}(q_{\theta^*} \parallel \hat{q}_k^{\text{com}}), \quad H_k^{\text{red}} \triangleq D_{KL}(q_{\theta^*} \parallel \hat{q}_k^{\text{red}}). \quad (15)$$

Since each q_θ is a product distribution over $\tilde{\Theta}$, see (12), the KL divergences may be expanded as

$$H_k^{\text{com}} = \sum_{\nu \in \{x, r, t\}} D_{KL}([q_{\theta^*}]_\nu \parallel \sum_{j \in \mathcal{P}} \omega_k^{(j)} [q_k^{(j)}]_\nu), \quad H_k^{\text{red}} = \sum_{\nu \in \{x, r, t\}} D_{KL}([q_{\theta^*}]_\nu \parallel \sum_{i \in \mathcal{M}_k} \frac{\omega_k^{(i)}}{\omega_{\text{eff}}} [q_k^{(i)}]_\nu). \quad (16)$$

Theorem 1. *The following lower bounds hold:*

$$\begin{aligned} H_k^{\text{com}} &\geq \underline{H}_k^{\text{com}} \triangleq -\log \left(\sigma_x^{1-n} \left(\frac{\mathbf{e}}{2} \right)^{\frac{n+2}{2}} \right) - \sum_{\nu \in \{x, r, t\}} \log \left(\sum_{j \in \mathcal{P}} \omega_k^{(j)} \mathbf{e}^{-\frac{\|\nu(\theta) - \nu(q_k^{(j)})\|^2}{4\sigma_\nu^2}} \right), \\ H_k^{\text{red}} &\geq \underline{H}_k^{\text{red}} \triangleq -\log \left(\frac{\sigma_x^{1-n}}{\omega_{\text{eff}}^3} \left(\frac{\mathbf{e}}{2} \right)^{\frac{n+2}{2}} \right) - \sum_{\nu \in \{x, r, t\}} \log \left(\sum_{i \in \mathcal{M}_k} \omega_k^{(i)} \mathbf{e}^{-\frac{\|\nu(\theta) - \nu(q_k^{(i)})\|^2}{4\sigma_\nu^2}} \right), \end{aligned} \quad (17)$$

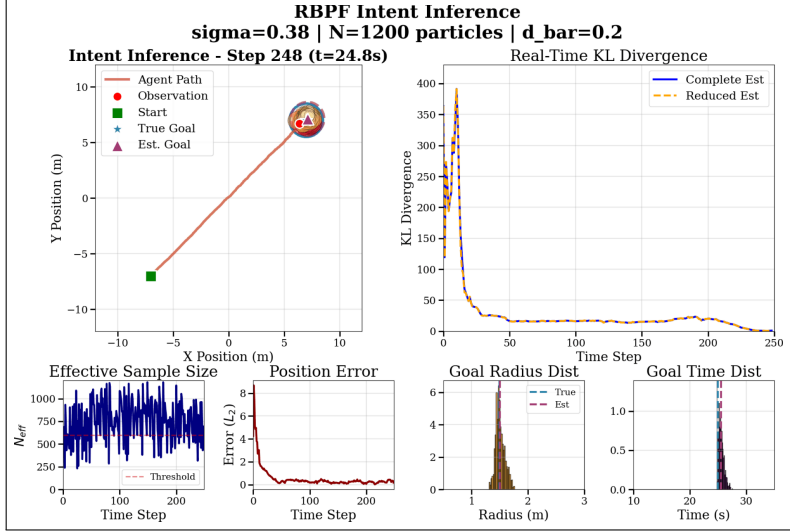


Figure 2: RBPF intent–inference process. The upper-left panel shows the agent’s trajectory, and the upper-right panel plots the KL divergence for the complete and reduced estimators. The four lower panels display, from left to right, the effective sample size N_{eff} , the position estimation error, the estimated goal radius, and the estimated arrival time.

and there exist constants C_x, C_r, C_t such that for all k :

$$\Delta H_k^{low} \triangleq |\underline{H}_k^{\text{com}} - \underline{H}_k^{\text{red}}| \leq \left| \sum_{\nu \in \{x, r, t\}} \left(\frac{1}{2} - \frac{1}{2\sqrt{2N}} \right) \log C_\nu \right|. \quad (18)$$

Proof. See Appendix B, where lower bounds on the C_ν are also derived, see Equation (30). \square

The lower bounds in (17) establish estimates of $\underline{H}_k^{\text{com}}$ and $\underline{H}_k^{\text{red}}$ in terms of data available to the adversary, in the absence of precise state information about the agent. The discrepancy between the lower bounds serves as a conservative metric for the difference in the performance of the two respective estimators, as formalized in (18).

5 Numerical Experiments

In this section, we evaluate the proposed RBPF for real-time intent inference in a planar goal-directed navigation task. The primary objective is to quantify the speed and accuracy with which the adversary can recover the agent’s hidden intent parameters $\theta^* = (x^*, r^*, t^*)$ using the derived density-based estimators.

5.1 Simulation Setup

The experiment takes place in a 2D domain where the agent starts randomly at $x_0 \in R\mathbb{B}$ with a true goal $\theta^* \in \Theta$ such that $\|x^* - x_0\| \geq 10$, $r^* \geq 1$ and $t^* \geq 20$. The agent follows the stable closed-loop dynamics in (2) with a disturbance bound $\bar{d} = 0.2$ and noise level $\sigma_d = 0.38$. The adversary employs an RBPF with $N = 1200$ particles initialized uniformly over the workspace. To rigorously measure the inference performance, we utilize the KL divergence in (16) as the primary metric of success. We define Inference Time (T_{inf}) as the time t_k at which the KL divergence drops below a threshold of $\epsilon = 50$ and remains bounded, indicating the adversary has successfully localized the intent distribution.

5.2 Results and Analysis

The simulation was repeated for 100 Monte Carlo trials. Figure 2 illustrates the inference process of the RBPF. Both estimators show an exponential decay in divergence as the agent moves toward the goal, reflecting the rapid reduction in uncertainty. Table 1 summarizes the terminal accuracy and inference speed, from which the Reduced Estimator consistently maintains lower final error states by pruning the ineffective particles. This result indicates that maintaining

Metric	Reduced Estimator	Complete Estimator
Inference Time	$3.28s \pm 2.28$	$3.28s \pm 2.28$
Final Position Estimation Error	$0.225m \pm 0.295$	$0.231m \pm 0.295$
Final Radius Estimation Error	$0.264m \pm 0.636$	$0.274m \pm 0.626$
Final Time Estimation Error	$0.729s \pm 0.699$	$0.732s \pm 0.697$

Table 1: Performance comparison of intent estimators with 100 times repeat experiments.

the complete estimator offers no information advantage over the reduced estimator, except possibly for rare cases (which are, at any rate, accounted for by the information leakage lower bound in Theorem 1).

At the very beginning of a trajectory, the posterior distribution is diffuse, with particles covering both candidate goals and exhibiting high variance. As the agent commits to a direction likelihood updates collapse the distribution around the correct goal, leading to rapid posterior concentration.

Across all runs, N_{eff} initially falls as weights become uneven, then rises after resampling, and oscillates during late-stage convergence. The position estimation error monotonically decreases as the particle cloud contracts around the true state trajectory. The predicted arrival-time histograms tighten as uncertainty shrinks, reflecting improved confidence in the inferred goal. The RBPF identifies the correct goal well before the halfway point of the trajectory, and the final estimate matches the ground truth with negligible error.

6 Conclusion

Intent inference for goal-directed motion as an RBPF over (x, r, t) were implemented, exploiting analytic Kalman updates to marginalize the linear–Gaussian part of the dynamics and thereby improving sample efficiency relative to standard particle filters. Density-based estimators of intent were developed, and the information leakage was evaluated using computable lower bounds to the KL divergence between the true intent distribution and estimator mixtures. Simulations demonstrate fast, accurate intent recovery despite noise. The framework separates control from inference and yields diagnostics with KL-bounds, and posterior marginals that are reproducible across tasks. Future work includes richer motion models and non-Gaussian observation channels, principled design of obfuscation controllers that minimize KL-based leakage subject to task constraints while keeping track of reference path, and extensions to multi-agent settings.

References

- [1] A. Kulkarni, M. Klenk, S. Rane, and H. Soroush. Resource bounded secure goal obfuscation. In *AAAI Fall Symp. Integr. Plan. Diagn. Causal Reason.*, 2018.
- [2] Sara Bernardini, Fabio Fagnani, and Santiago Franco. An optimization approach to robust goal obfuscation. In *Int. Conf. Princ. Knowl. Represent. Reason.*, pages 119–129, 2020.
- [3] Peta Masters and Sebastian Sardina. Deceptive path-planning. In *Int. Jt. Conf. Artif. Intell. (IJCAI)*, page 4368–4375, 2017.
- [4] Yagiz Savas, Melkior Ornik, Murat Cubuktepe, Mustafa O Karabag, and Ufuk Topcu. Entropy maximization for markov decision processes under temporal logic constraints. *IEEE Trans. Autom. Control*, 65(4):1552–1567, 2019.
- [5] Michael Hibbard, Yagiz Savas, Zhe Xu, and Ufuk Topcu. Minimizing the information leakage regarding high-level task specifications. *IFAC-PapersOnLine*, 53(2):15388–15395, 2020.
- [6] Parham Gohari, Matthew Hale, and Ufuk Topcu. Privacy-preserving policy synthesis in Markov Decision Processes. In *IEEE Conf. Decis. Control (CDC)*, pages 6266–6271, 2020.
- [7] Austin Jones, Kevin Leahy, and Matthew Hale. Towards differential privacy for symbolic systems. In *Am. Control Conf. (ACC)*, pages 372–377, 2019.
- [8] Bo Chen, Kevin Leahy, Austin Jones, and Matthew Hale. Differential privacy for symbolic systems with application to Markov Chains. *Automatica*, 152:110908, 2023.
- [9] Timothy L Molloy and Girish N Nair. Smoother entropy for active state trajectory estimation and obfuscation in pomdps. *IEEE Trans. Autom. Control*, 68(6):3557–3572, 2023.
- [10] Kevin Murphy and Stuart Russell. Rao-Blackwellised particle filtering for dynamic bayesian networks. In *Seq. Monte Carlo methods pract.*, pages 499–515. Springer, 2001.

- [11] M.S. Arulampalam, S. Maskell, N. Gordon, and T. Clapp. A tutorial on particle filters for online nonlinear/non-gaussian bayesian tracking. *IEEE Trans. Signal Process.*, 50(2):174–188, 2002.
- [12] Graeme Best and Robert Fitch. Bayesian intention inference for trajectory prediction with an unknown goal destination. In *IEEE/RSJ Int. Conf. Intell. Robots Syst. (IROS)*, pages 5817–5823, 2015.
- [13] J. P. Aubin and H. Frankowska. *Set-valued analysis*. Birkhäuser, 2008.
- [14] J.-L. Durrieu, J.-Ph. Thiran, and F. Kelly. Lower and upper bounds for approximation of the Kullback-Leibler divergence between Gaussian Mixture Models. In *IEEE Int. Conf. Acoust. Speech Signal Process. (ICASSP)*, pages 4833–4836, 2012.
- [15] Yixuan Wang, Dan Guralnik, Saiedeh Akbari, and Warren Dixon. Effective model pruning. *arXiv preprint arXiv:2509.25606*, 2025.

A Proof of Lemma 1

Let $e \triangleq x - x(\theta)$ denote the error state and consider the Lyapunov function candidate $V(e) \triangleq \|e\|^2$. Following [13, Theorem 10.1.3], let $x : [0, T] \rightarrow \mathbb{R}^n$, $T \in (0, \infty]$ be a complete solution of the differential inclusion (3). Applying the chain rule to the composition $V \circ e$ and noting that V is a smooth function yields

$$\dot{V} \in 2e^\top (-\lambda e + \bar{d}\mathbb{B}) = -2\lambda V + 2\bar{d}e^\top \mathbb{B}, \quad (19)$$

for almost all t . Hence,

$$\dot{V} \leq -2\lambda V + 2\bar{d}V^{\frac{1}{2}} \text{ a. e. } ([0, T]). \quad (20)$$

Multiplying both sides of (20) by $V^{1/2} \exp(\lambda t)$ and integrating yields, after some algebra:

$$V(e(t))^{\frac{1}{2}} \leq V(e(0))^{1/2} e^{-\lambda t} + \frac{\bar{d}}{\lambda} (1 - e^{-\lambda t}) \quad (21)$$

Using $\|e(0)\| \leq R$ and $V^{\frac{1}{2}} = \|e\|$ results in

$$\|e\| \leq R e^{-\lambda t} + \frac{\bar{d}}{\lambda} (1 - e^{-\lambda t}). \quad (22)$$

To ensure $\|e\| \leq r(\theta)$ for all $t > t(\theta)$, it is required that:

$$R e^{-\lambda t} + \frac{\bar{d}}{\lambda} (1 - e^{-\lambda t}) \leq r(\theta), \quad (23)$$

which is equivalent to

$$\lambda \left(1 - \frac{R}{r(\theta)} e^{-\lambda t} \right) \geq \frac{\bar{d}}{r(\theta)} (1 - e^{-\lambda t}), \quad (24)$$

It follows from (4) that the second factor on the left-hand side of (24) is positive for all $t > t(\theta)$. Therefore, (24) is equivalent to:

$$\lambda \geq \frac{\bar{d}}{r(\theta)} \frac{1 - e^{-\lambda t}}{1 - \frac{R}{r(\theta)} e^{-\lambda t}}, \quad (25)$$

Note that $\frac{R}{r(\theta)} > 1$, by (1). Furthermore, the function $K_B(a) \triangleq \frac{1-B}{1-aB}$ is decreasing in the interval $[1, \infty)$ for any $B \in (0, 1)$. In particular, $K_{e^{-\lambda t}}(\frac{R}{r(\theta)}) \leq K_{e^{-\lambda t}}(1) = 1$. Therefore, to guarantee (25) it suffices for λ to satisfy $\lambda \geq \bar{d}/r(\theta)$, which is provided by 4.

B Proof of Theorem 1

Applying lower bounds for KL-divergences between a single Gaussian and a Gaussian mixture model (GMM) from [14] yields lower bounds for each term. For example, a lower bound for the x term in the reduced estimator of (16) is

$$D_{KL} \left([q_{\theta^*}]_x \middle\| \sum_{i \in \mathcal{M}_k} \frac{\omega_k^{(i)}}{\omega_{\text{eff}}} [q_k^{(i)}]_x \right) \geq -\log \left(\sum_i \omega_k^{(i)} e^{-\frac{\|x(\theta) - x(q_k^{(i)})\|^2}{4\sigma_x^2}} \right) - \log \left(\frac{\sigma_x^{1-n}}{\omega_{\text{eff}}} \frac{e^{\frac{n}{2}}}{2} \right). \quad (26)$$

where n denotes the dimension of the position $x(\theta)$; in this paper, as stated in Section 2, we restrict attention to $n \in 2, 3$. Collecting all three terms together amounts to the lower bound $\underline{H}_k^{\text{com}}$ and $\underline{H}_k^{\text{red}}$. Upper bounds similar to (17) exist, from which a convergence analysis of the information can be derived in future work. We proceed to analyze ΔH_k^{low}

$$\Delta H_k^{\text{low}} = |\underline{H}_k^{\text{com}} - \underline{H}_k^{\text{red}}| = \left| \sum_{\nu \in \{x, r, t\}} \log \left(\frac{\omega_{\text{eff}} \frac{\sum_{j \in \mathcal{P}} \omega_k^{(j)} e^{-\frac{\|\nu(\theta) - \nu(q_k^{(j)})\|^2}{4\sigma_\nu^2}}}{\sum_{i \in \mathcal{M}_k} \omega_k^{(i)} e^{-\frac{\|\nu(\theta) - \nu(q_k^{(i)})\|^2}{4\sigma_\nu^2}}}} \right) \right|, \quad (27)$$

Define the function $f(\nu)$ and d_ν as follows:

$$f(\nu) \triangleq \frac{\sum_{j \in \mathcal{P} \setminus \mathcal{M}_k} \omega_k^{(j)} d_\nu}{\sum_{i \in \mathcal{M}_k} \omega_k^{(i)} d_\nu}, \quad d_\nu \triangleq e^{-\frac{\|\nu(\theta) - \nu(q_k^{(j)})\|^2}{4\sigma_\nu^2}} \quad (28)$$

The constraint $\theta \in \Theta$ implies:

$$d_x \geq e^{-\frac{R^2}{\sigma_\nu^2}}, \quad d_r \geq e^{-\frac{\|r_{\max} - r_{\min}\|^2}{4\sigma_\nu^2}}, \quad d_t \geq e^{-\frac{\|T_{\max} - T_{\min}\|^2}{4\sigma_\nu^2}}, \quad (29)$$

which motivates defining

$$\underline{d}_x \triangleq e^{-\frac{R^2}{\sigma_\nu^2}}, \quad \underline{d}_r \triangleq e^{-\frac{\|r_{\max} - r_{\min}\|^2}{4\sigma_\nu^2}}, \quad \underline{d}_t \triangleq e^{-\frac{\|T_{\max} - T_{\min}\|^2}{4\sigma_\nu^2}}. \quad (30)$$

Therefore, an upper bound on $f(\nu)$ is derived

$$f(\nu) = \frac{\sum_{j \in \mathcal{P} \setminus \mathcal{M}_k} \omega_k^{(j)} d_\nu}{\sum_{i \in \mathcal{M}_k} \omega_k^{(i)} d_\nu} \leq \frac{\sum_{j \in \mathcal{P} \setminus \mathcal{M}_k} \omega_k^{(j)}}{C_\nu \cdot \sum_{i \in \mathcal{M}_k} \omega_k^{(i)}} = \frac{1 - \omega_{\text{eff}}}{C_\nu \omega_{\text{eff}}}, \quad (31)$$

where $C_\nu \triangleq \min_{i \in \mathcal{M}_k} d_\nu \in [\underline{d}_\nu, 1]$. Similarly,

$$f(\nu) \geq \frac{1 - \omega_{\text{eff}}}{\omega_{\text{eff}}} B_\nu, \quad (32)$$

where $B_\nu \triangleq \min_{i \in \mathcal{P} \setminus \mathcal{M}_k} d_\nu \in [\underline{d}_\nu, 1]$. Then the additional information ΔH_k^{low} is upper bounded by:

$$\Delta H_k^{\text{low}} = \left| \sum_{\nu \in \{x, r, t\}} \log(\omega_{\text{eff}}(1 + f(\nu))) \right| \leq \left| \sum_{\nu \in \{x, r, t\}} (1 - \omega_{\text{eff}}) \log C_\nu \right|,$$

and the additional information ΔH_k^{low} is lower bounded by:

$$\Delta H_k^{\text{low}} \geq \left| \sum_{\nu \in \{x, r, t\}} \log(\omega_{\text{eff}} + (1 - \omega_{\text{eff}}) B_\nu) \right| \quad (33)$$

Proposition 2 ([15, Section 4.2]). *If $N_{\text{eff}} = 1$ then $\omega_{\text{eff}} \geq \frac{1}{2}$. If $N_{\text{eff}} = N$ then $\omega_{\text{eff}} = 1$. Otherwise,*

$$\omega_{\text{eff}} \geq \frac{N_{\text{eff}}}{N} + \frac{N - N_{\text{eff}}}{N} \sqrt{\frac{N - N_{\text{eff}} - 1}{(N_{\text{eff}} + 1)(N - 1)}}. \quad (34)$$

The bounds are sharp.

Then, apply Proposition 2 on ω_{eff} , the bound for the effective weight becomes $\omega_{\text{eff}} \in [(1 + \frac{1}{\sqrt{2N}})/2, 1]$. Hence, the additional information ΔH_k^{low} can be bounded by:

$$0 \leq \Delta H_k^{\text{low}} \leq \left| \sum_{\nu \in \{x, r, t\}} \left(\frac{1}{2} - \frac{1}{2\sqrt{2N}} \right) \log C_\nu \right|. \quad (35)$$